JACS
JOURNAL OF THE AMERICAN CHEMICAL SOCIETY
Article
pubs.acs.org/JACS

Mechanochemistry of One-Dimensional Boron: Structural and Electronic Transitions

Mingjie Liu,[†] Vasilii I. Artyukhov,*[,†] and Boris I. Yakobson*

Department of Materials Science & NanoEngineering, and Department of Chemistry, Rice University, Houston, Texas 77005, United States

Supporting Information

ABSTRACT: Recent production of long carbyne chains, concurrent with advances in the synthesis of pure boron fullerenes and atom-thin layers, motivates an exploration of possible one-dimensional boron. By means of first-principles calculations, we find two isomers, two-atom wide ribbon and single-atom chain, linked by a tension-driven (negative-pressure) transformation. We explore the stability and unusual properties of both phases, demonstrating mechanical stiffness on par with the highest-performing known nanomaterials, and a phase transition between stable 1D metal and an antiferromagnetic semiconductor, with the phase boundary effectively forming a stretchable 1D Schottky junction. In addition, the two-phase system can serve as a constant-tension nanospring with a well-calibrated tension defined by enthalpic balance of the phases. Progress in the synthesis of boron nanostructures suggests that the predicted unusual behaviors of 1D boron may find powerful applications in nanoscale electronics and/or mechanical devices.

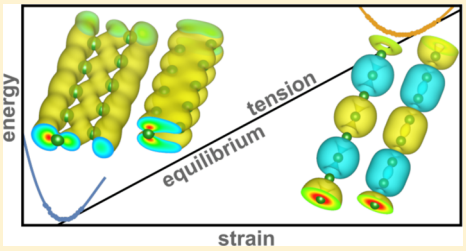

1. INTRODUCTION

Carbon nanostructures have spearheaded a number of advances in chemistry and materials,[1] beginning with fullerenes and nanotubes.[2] More recently, graphene has created a boom of research.[3] Another exotic form of carbon, one-dimensional chains, also known as carbyne, has been a subject of scientific controversy since the 1960s, but with the advent of more powerful synthetic and measuring techniques, it is becoming more accessible,[4,5] and most recently was produced in quantity, in a stable encapsulated form.[6] Meanwhile, boron nanostructures are being actively investigated. Boron fullerenes were theoretically proposed,[7] and more recently synthesized experimentally, in a smaller size.[8,9] Atomically thin 2D films have long since been predicted theoretically,[10−13] culminating in recent experimental syntheses.[14−19] Evidence for elongated ribbon-like $B_{4n}H_2$ clusters,[20] tubular B_{20} clusters,[21,22] as well as transition metal centered circular boron ribbon clusters[23,24] have also been reported.[20−24] In the context of this remarkable progress, one naturally wonders what the structure and properties of 1D boron nanostructures could eventually look like, especially because for carbon, the 1D form is expected to have most extreme properties both mechanically and electronically.[25−28] As we demonstrate in the present first-principles theoretical study, 1D boron indeed has a fascinating combination of properties, including a chemomechanics of tensile strain controlled isomerization,[29] a reversible structural phase transition between metallic and wide-gap semiconducting forms under tension.

2. COMPUTATIONAL DETAILS

Density functional theory calculations were performed using the VASP code.[30,31] Most calculations used the PBE[32,33] exchange-correlation functional. Where indicated, the HSE06 hybrid functional[34,35] was used to improve the accuracy of structural distortions and associated band gaps. Projector-augmented wave basis set was used[36,37] with a cutoff of 400 eV. Structural relaxation was performed until all forces were less than 0.01 eV/Å. At least 10 Å vacuum spacing was maintained in the nonperiodic directions. Climbing-image nudged elastic band[38] calculations to locate transition states were performed with five images between initial and final structures. Density-functional tight binding calculations were done with the DFTB+ code[39] using Slater−Koster parameters from ref 40 at a temperature of 2000 K with 1 fs time step and a 5 ps runtime between sequential 1% engineering strain increments, with total time approaching ∼1 ns. The model system contained 64 atoms.

3. RESULTS AND DISCUSSION

3.1. Phases of One-Dimensional Boron. Calculations by others[41] show that, for boron, a carbyne-like linear chain (henceforth denoted as C) structure has higher energy than a ribbon-like (R) structure with two staggered atomic rows. Therefore, the C structure is less stable in tension-free mechanical equilibrium. However, the two structures have a 2-fold difference in linear density (Figure 1a,d). From this, we can hypothesize that external tension can stabilize C over R, using mechanical work to overcome the energy difference. In this study, we show that this mechanically driven phase transition is indeed possible, in the sense that (1) it is energetically preferred to trivial breaking of R; (2) it is reversible; and (3) it happens on practically useful time scales. Before discussing these findings in detail, we explore the remarkably different electronic and mechanical properties of

Received: December 12, 2016
Published: January 18, 2017

DOI: 10.1021/jacs.6b12750
J. Am. Chem. Soc. 2017, 139, 2111−2117

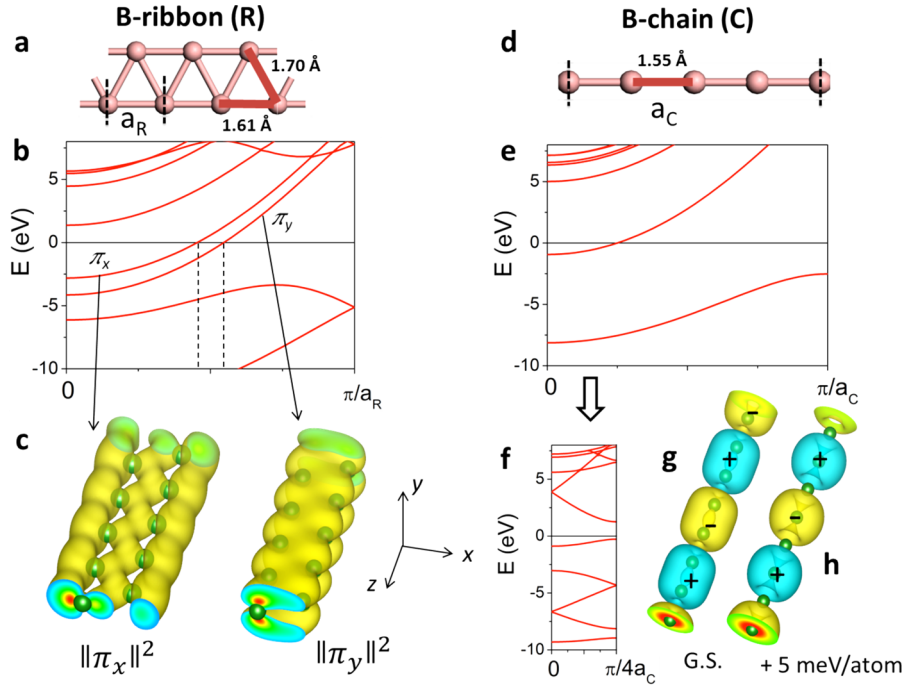

Figure 1. Electronic structure of 1D boron ribbons and chains. Ribbons (a) have two nondegenerate Fermi wavevectors (see band structure in b) stemming from broken π-band symmetry (spatial distributions of corresponding electron densities shown in (c)), which prevents Peierls transition from opening a band gap. Chains (d) undergo an antiferromagnetic transition with a 4-cell spin density wave (SDW) period (band structure e → f) with two almost-degenerate solutions: a bond-SDW ground state (g) and a site-SDW 5 meV/atom higher state (h).

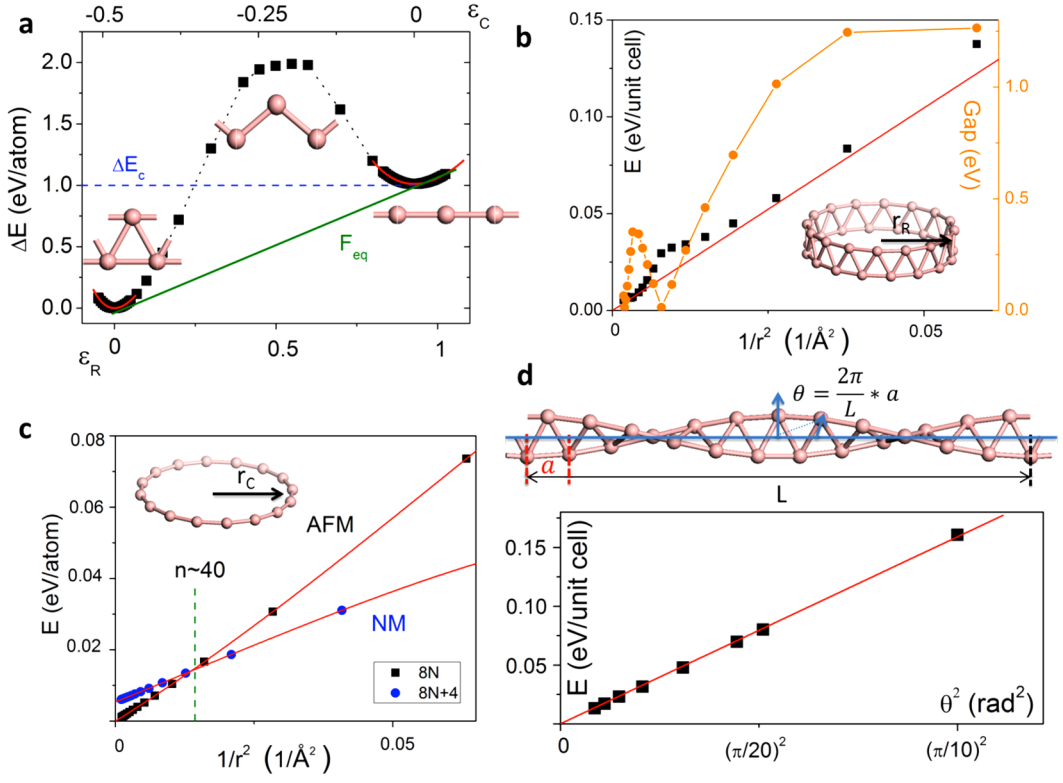

Figure 2. Mechanics of one-dimensional boron. (a) Energy–strain curve showing two distinct minima for ribbons (R) and chains (C). The equilibrium tension F_{eq} is defined as the common tangent for the two minima. The curvature of the plot in the minima yields tensile stiffness of the phases, and the maximum slope provides an estimate of breaking strength. (b) Bending stiffness of R phase as calculated using a ring model. The "■" and orange "●" represent the energy and band gap, respectively. The nonlinearities around curvature values result from the degeneracies between different-symmetry of π orbitals during bending. (c) Ring model calculations for bending stiffness of C phase, with alternating antiferromagnetic (AFM) and nonmagnetic (NM) ground-state solutions. (d) Twisting of the R phase for torsional stiffness fitting.

DOI: 10.1021/jacs.6b12750
J. Am. Chem. Soc. 2017, 139, 2111−2117

the two phases separately. While we cannot confidently rule out other 1D structures, our efforts to detect thicker wire-like phases with triangular or square cross-section (structures can be found in the Supporting Information) have failed to find any simple candidate structures with energy lower than that of R. The phonon dispersion (see the Supporting Information) of both phases also provides the evidence for the stability of those 1D structures.

3.2. Electronic Structure of Chains and Ribbons. The R structure is convenient to think of as an infinite extension of previously observed ribbon-like clusters.[20,21] The chemistry of the latter is analogous to linear carbon with every rhombic B_4 unit playing the role of a C_2 unit because boron has one-half as many π electrons per atom.[42,43] One might conclude that a perfectly symmetric R structure must be a metal with half-band filling in each of the two π bands, which appears to fulfill the conditions of Peierls theorem[44−47] and thus should spontaneously tetramerize, as carbyne's cumulene structure is predicted to dimerize,[48] in the fixed-nuclei approximation. However, unlike in carbyne, the planar, instead of the axial, symmetry of R breaks the degeneracy of π_x and π_y bands (shown in Figure 1c). As a result, the bands are split, and the system has two Fermi wavevectors (Figure 1b), neither lying at Brillouin zone middle, yielding no charge-density waves (CDW) commensurate with reasonably small-size supercell and hence the absence of any detectable structural rearrangement.

The C structure (Figure 1d) has one fewer π electron per atom than carbyne and thus can be interpreted as carbyne with 1/4 band filling (Figure 1e). As a result, one would expect again a Peierls tetramerization with a $\pi/4a$ CDW period. Instead, however, our calculations show the formation of a spin-density wave (SDW) with almost no atomic rearrangement (Figure 1f). We identified two stable solutions: a bond-SDW (↑↑↓↓) and site-SDW (↑•↓•) as shown in Figure 1g,h, respectively, with the latter 5 meV/atom higher in energy (HSE functional) and strictly zero bond length alternation due to symmetry, and the bond-SDW state showing a negligibly weak dimerization. The band gap of the bond-SDW is 1.52 eV (HSE). As expected for all similar 1D systems,[27] stretching increases the band gap to 1.76 eV at 10% strain, which is appreciable although not as dramatic as carbyne CDW.[25,27] The gap increase here is not due to electron−phonon coupling[27] but rather an increased SDW amplitude, which grows from 0.25 μ_B per atom to 0.3 μ_B at 10% strain.

3.3. Mechanics of One-Dimensional Boron. The most basic property of any solid material is its resistance to deformation. In this section, we calculate the elastic moduli to demonstrate that R and C phases are true stable materials with distinct mechanics.

The calculation of tensile stiffness is shown in Figure 2a. As the unit cell size is scaled, we observed two distinct minima separated by ΔE_c = 1 eV, which is the cohesive energy difference between the two phases. The curvature of each minimum defines the tensile stiffness of its corresponding phase. We calculated the stiffness to be 72 and 46 eV/Å, which is about 3/4 and 1/2 of that for carbyne, for R and C phases, respectively. However, the lattice constant of C-boron is about 20% larger than that of carbyne, and the atomic weight is a further 10% smaller, which brings the specific stiffness of C-boron to 6.4 × 10^8 Nm/kg, almost 2/3 of carbyne's value. At the same time, the twice-higher linear density of the R phase makes it the softer one of the two on a per-mass basis (5.2 × 10^8 Nm/kg, about one-half of carbyne).

The hill between the two energy minima is the primary direct evidence of the phase transition. If we start with the R structure and stretch it to some point on the black curve in Figure 2a between the minima, for a large sample it will always be favorable to separate into R and C regions instead of stretching uniformly, with the total energy being lowered to the green straight line. The latter is defined as the common tangent of the two potential wells, and its slope yields the equilibrium tension F_{eq} = 2.13 nN. This is the value at which both phases have identical enthalpy, $H = E + FL$. Above it, R has higher enthalpy and thus gets converted into C, and vice versa. Under fixed-length boundary conditions between the two tangent points, the system will relax toward an R−C mixture in such proportions that the tension equals F_{eq}. It thus behaves as a fixed-tension nanospring with a stretching range of about 100%.

By taking the slope of the Figure 2a plot at the inflection points of energy−strain curves, we can estimate the ideal breaking strength of the phases, yielding 7.38 and 9.73 nN for C and R, respectively. These values correspond to 64 × 10^6 and 44 × 10^6 Nm/kg specific strength, respectively (85% and 60% of carbyne). Importantly, F_{eq} is well below both breaking points.

To calculate the bending stiffness, as before,[25] we use rings of increasing radius (decreasing curvature) to extract the $E(1/r^2)$ asymptote slope, where E is the energy of ring with radius r. When plotted in respective coordinates, the energy E_R of R "nanobelts" (Figure 2b) shows a strikingly nonlinear behavior. The upward deviation from the straight line in Figure 2b turns out to be again rooted in symmetries. Because of the different spatial distributions of π_x and π_y bands (Figure 1c), they strongly differ in susceptibility to curvature. More specifically, the π_y band, which is the lower-energy one for the flat structure, is much more extended in the direction of curvature, and thus its energy increases faster with bending, necessarily crossing over the π_x band. This point is marked by the almost-zero HOMO−LUMO gap of the ring (B_{44}) and an increased bending stiffness. This behavior repeats at lower curvatures, perhaps due to "tune-in" of other bands of π_y and π_y character with each other. A detailed analysis of ring molecular orbitals is presented in the Supporting Information. To get an estimate of the bending stiffness of the infinite R phase, we computed the stiffness for each value of r based on ring energy $E_R(r)$ and the cohesive energy of the infinite ribbon $E_R(\infty)$, and took the lowest value, 2.6 eV Å, which yields a persistence length of 10 nm at room temperature, roughly on par with carbyne.[25]

The C phase of boron also at first seems to behave extremely nonlinearly when curved into rings as seen in Figure 2c. However, the oscillatory behavior is easily understood by dividing the rings into two families, B_{8N} and B_{8N+4}, with $E_C(r)$ for each perfectly following the predicted asymptotic of $\sim 1/r^2$. This situation is analogous to the first-/second-order Jahn−Teller effect in carbyne rings.[25,49] Interestingly, the ground state of B_{8N+4} rings is nonmagnetic. The intersection of the two lines in Figure 2c (around B_{40}) thus can be interpreted as a "curvature-induced magnetic transition". The stiffness is 0.81 eV Å for nonmagnetic rings (low-curvature asymptotic) and 1.25 eV Å for antiferromagnetic, the latter corresponding to a room-temperature persistence length of 4.9 nm.

Finally, the planar symmetry of R structure makes it possible to define a torsion stiffness without a need for symmetry-breaking "handles".[25] The model system, illustrated in Figure

DOI: 10.1021/jacs.6b12750
J. Am. Chem. Soc. 2017, 139, 2111−2117

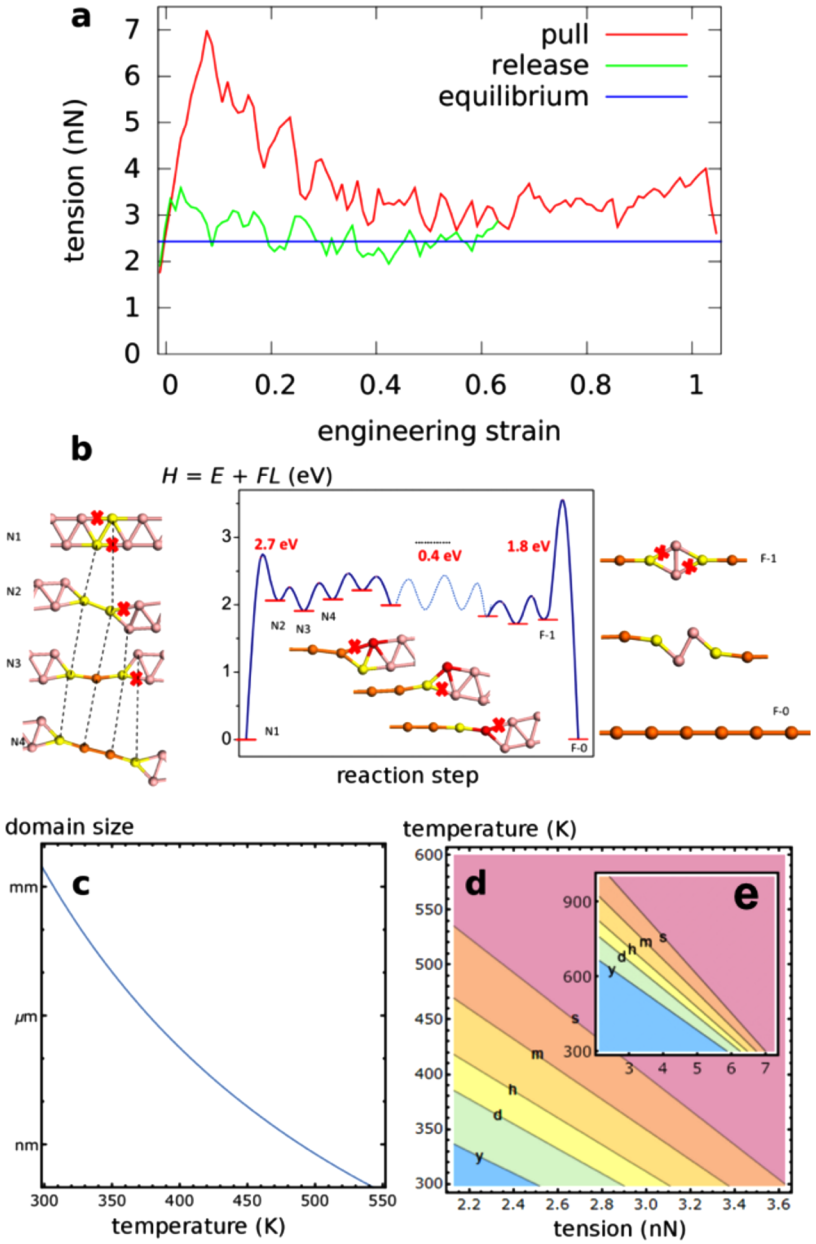

Figure 3. Ribbon−chain, R ↔ C phase transition. (a) Evolution of tension in molecular dynamics simulations of stretching (including reversal); see Supporting Videos. (b) Enthalpy variation over sequential steps of R−C phase transition under equilibrium tension. The corresponding structures are shown with a red "×" marking sequential bond breakings. (c) Domain length (inverse concentration of R|C and C|R interfaces) in 1D boron under thermal and mechanical equilibrium. (d) Ductility diagram showing contours of phase transition time scales, from (s)econds to (y)ears, as a function of temperature and tension, assuming nucleation at ribbon ends; that is, the activation barrier used is one-half of the 2.7 eV (b) value. The inset (e) shows a full-barrier estimate corresponding to "homogeneous" midribbon nucleation of C phase.

2d, consists of a supercell in which the ribbon makes a 360° twist. By varying the supercell size, we can calculate the energy as a function of twist per unit cell and determine the stiffness by extrapolation, yielding a value of ∼5 eV Å, about 1/2 of the value for carbyne.

Similarly to previous work on carbyne,[25] we can use the calculated properties to define equivalent continuum elastic models for both phases. With the cylindrical rod representation for C-boron, we find a nominal Young's modulus of Y_C = 21.6 TPa at a nominal thickness (diameter) of $2r_C$ = 0.66 Å. For simplicity, we approximate the R phase as a rectangular "plank" of thickness t and width b = 1.5 Å, and the system of equations governing the elastic behavior is then

$$C = \frac{1}{a_R^2}\frac{\partial^2 E}{\partial \varepsilon^2} = \frac{btY}{a_R}$$

$$K = \frac{1}{a_R}\frac{\partial^2 E}{\partial\left(\frac{1}{R}\right)^2} = \frac{1}{12}bt^3Y$$

$$H = a_R\frac{\partial^2 E}{\partial \theta^2} = J\cdot G$$

Here, J is the torsional constant approximately given by $J = bt^3\left[\frac{1}{3} - 0.21\frac{t}{b}\left(1 - \frac{t^4}{12b^4}\right)\right] \approx 0.1$ Å^4.[50] Solving the sys-

DOI: 10.1021/jacs.6b12750
J. Am. Chem. Soc. 2017, 139, 2111−2117

tem yields an effective thickness of t = 0.658 Å, Young's modulus of Y = 11.7 TPa, and a shear modulus of G = 8 TPa. (The corresponding crudely defined Poisson's ratio is −0.27.) In sum, while the nominal elastic moduli for 1D boron are smaller than those for carbyne,[25] they are still very high, once again emphasizing the unusual mechanical properties of one-dimensional nanomaterials.

3.4. Chain−Ribbon Phase Transition. Having characterized the R and C phases of 1D boron as stand-alone phases with their own remarkable and very distinct properties, we now proceed to study the phase transformation that connects them. To check whether it is at all possible, we first performed a molecular dynamics simulation of stretching a 64-atom R supercell with the density-functional tight binding (DFTB) method. Under such stretching, the system gradually underwent a smooth transition into the C phase via a series of nucleation events followed by interface propagation (see Supporting Video 1). We observed multiple interface nucleation resulting from the high temperature, as explained below. Upon collisions of C|R and R|C interfaces as an R domain shrank, we observed formation of rhomb-shaped "knots", which would persist almost to the end of the stretching run. We also performed a reverse simulation starting from the structure at 65% elongation (chosen so as to have a fragment of R phase still intact to serve as a "seed"-nucleus) and gradually released to contract to original length. The trajectory in Supporting Video 2 shows growth of R structure at the expense of C-portion back to the original all-R structure. During both molecular dynamics runs, we monitored the average tension for each elongation value (Figure 3a). The stretching run shows an initial "overstretching" behavior indicative of a nucleation event, and then remains effectively constant up to full stretching. Compression is also accompanied by a constant (and somewhat lower) tension value. The equilibrium tension computed as in Figure 2a but using DFTB is 2.43 nN, close to the DFT value and in excellent agreement with the tension value during molecular dynamics compression.

Our molecular dynamics simulations validate the prediction of an R−C phase transition in 1D boron under tension, even at the rather high strain rates and temperatures required imposed by computational resource limitations. Therefore, it is compelling to study the phase transition kinetics under more relevant conditions of lower strain rates and temperatures. With that aim, we calculated step-by-step energies and activation barriers for the transformation of R into C using a 24-atom supercell. The calculations are performed under constant tension corresponding to phase equilibrium, where the relevant thermodynamic quantity is the enthalpy $H = E + FL$. While it is easy to perform variable-cell geometry relaxations to ensure exactly the right tension, the problem of locating transition states becomes much more difficult under constant-tension boundary conditions. We thus adopted a grid-search approach. We performed fixed-cell transition state searches (using manual scan with a suitable choice of reaction coordinate or with the climbing-image nudged elastic band method, further refined by the dimer method) with different cell lengths chosen so as to ensure that the transition states thus located do bracket the equilibrium tension. The energy (enthalpy) barrier under equilibrium tension then was determined using interpolation. This approach enables us to not only compute the kinetics of phase transition under equilibrium tension, but further to directly evaluate how the kinetic barriers are affected by loads above or below equilibrium.

We find that the nucleation of C structure (N1−N2−N3−N4 in Figure 3b) is limited by the first bond-breaking event with a 2.7 eV barrier. After that, the enthalpy quickly sets into a repetitive pattern with a period of 4 and a maximum barrier height of 0.4 eV within a period, which corresponds to interface propagation. The periodic behavior can be considered as an artifact of a finite model system due to electron-counting rules for bond conjugation,[42,43] and in an idealized system with two semi-infinite phases there would be no such oscillation.

By averaging the energies of states in the propagation part and dividing by two (number of interfaces in the model system), we can estimate the free energy (enthalpy) of a single R|C interface as $H^* = 1.0 \pm 0.07$ eV. On the basis of this, we can evaluate the concentration c of domain interfaces in mechanical and thermal equilibria as a function of temperature, so that $c^{-1} \approx a_R \exp(H^*/k_BT)$. As Figure 3c shows, the interface energy is large enough that at room temperature one should expect millimeter-scale coherent phase domains. As the temperature increases, we gradually enter the conditions where the system is expected to become a homogeneous mixture of small nanometer-scale domains, at temperatures above ∼500 K. This is consistent with multiple nucleation sites seen in the Supporting Videos.

Finally, from kinetic barriers, we can estimate the speed of the phase transition. Knowing not only the values of barriers but also how they react to changes in tension, we can construct the contour diagram in Figure 3d. The horizontal axis shows the tension (the left boundary is the equilibrium value of 2.13 nN), the vertical axis shows temperature T, and contours denote the levels where the frequency of crossing the nucleation barrier per unit cell length is one per time unit: (y)ear, (d)ay, (h)our, (m)inute, and (s)econd. The frequency is estimated as $f = 10^{13} \exp[-\delta H^*(F)/k_BT]$ where $\delta H^*(F)$ is the interpolated activation barrier height at tension F, and the prefactor is on the order of k_BT/h.[51] The mobility of the interface can be similarly estimated (assuming unilateral motion) by substituting $\delta H^*(F)$ with the periodic oscillation barrier ∼0.4 eV and multiplying the resulting frequency by a_R. This yields values on the millimeter-per-second order at 300 K.

4. CONCLUSIONS

The arguments against the possibility of phases in 1D are well-known. Despite that, our present calculations show that on practically relevant time- and length-scales boron forms two well-defined phases, chains and ribbons isomeric forms. The two phases are linked by a reversible phase transition. The dynamics of the transition can be tuned over many orders of magnitude by external tension and temperature. Each isomer by itself has formidable mechanical properties with different interesting nonlinearities. Further, one (ribbon) is a true 1D metal robust against Peierls distortion, and the other (chain) is a strain-tunable wide-gap antiferromagnetic semiconductor. Thus, electronically the two-phase system represents a stretchable Schottky junction, while from the mechanics standpoint it is a constant-tension spring with a fundamentally fixed tension value of 2.13 nN. This diversity of behaviors of 1D boron is certainly remarkable from the fundamental standpoint, and may lead to interesting novel electromechanical applications. Although speculating on the synthetic routes of making 1D boron is beyond the scope of the current study, one can envisage the chains pulled from borophene fragments (similar to the carbon or BN case[26,28,41]), or B-chains forming along the steps of the vicinal substrate surfaces; also, the boron−boron

DOI: 10.1021/jacs.6b12750
J. Am. Chem. Soc. 2017, 139, 2111−2117

coupling reaction[52] can be a promising path toward making 1D boron ribbons or chains. Finally, other chemical compositions such as silicon were found to also permit R-like structures in 1D,[53] and our analysis straightforwardly generalized to all of these materials as well.

■ ASSOCIATED CONTENT

Supporting Information

The Supporting Information is available free of charge on the ACS Publications website at DOI: 10.1021/jacs.6b12750.

Supporting Figures S1−S4, Tables S1 and S2, and videos S1 and S2; details of transition state barrier calculation and discussion of boron ribbon ring molecular orbitals, the structures and energies of possible wire-like 1D boron phases, and phonon dispersion of B-ribbon and B-chain (PDF)

Video of DFTB MD simulations (AVI)

Video of DFTB MD simulations (AVI)

Optimized structure data for helix wire-like 1D-boron phase (CIF)

Optimized structure data for linear chain 1D-boron phase (CIF)

Optimized structure data for parallel wire-like 1D-boron phase (CIF)

Optimized structure data for ribbon 1D-boron phase (CIF)

Optimized structure data for triangular wire 1D-boron phase (CIF)

■ AUTHOR INFORMATION

Corresponding Authors

*artyukhov@phystech.edu

*biy@rice.edu

ORCID

Mingjie Liu: 0000-0002-5341-4448

Author Contributions

†M.L. and V.I.A. contributed equally to this work.

Notes

The authors declare no competing financial interest.

■ ACKNOWLEDGMENTS

This work was supported by the Office of Naval Research grant N00014-15-1-2372 and by the Robert Welch Foundation (C-1590). The computational resources were provided by DAVinCI cluster funded by NSF. M.L. thanks Henry Yu for the helpful discussion on boron ribbon ring molecular orbitals.

■ REFERENCES

(1) Penev, E. S.; Artyukhov, V. I.; Ding, F.; Yakobson, B. I. *Adv. Mater.* **2012**, *24* (36), 4956−4976.

(2) Dresselhaus, M. S.; Dresselhaus, G.; Eklund, P. C. *Science of Fullerenes and Carbon Nanotubes: Their Properties and Applications*; Academic Press: San Diego, CA, 1996.

(3) Novoselov, K. S.; Fal'ko, V. I.; Colombo, L.; Gellert, P. R.; Schwab, M. G.; Kim, K. *Nature* **2012**, *490* (7419), 192−200.

(4) Banhart, F. *Beilstein J. Nanotechnol.* **2015**, *6*, 559−569.

(5) Casari, C. S.; Tommasini, M.; Tykwinski, R.; Milani, A. *Nanoscale* **2016**, *8*, 4414−4435.

(6) Shi, L.; Rohringer, P.; Suenaga, K.; Niimi, Y.; Kotakoski, J.; Meyer, J. C.; Peterlik, H.; Wanko, M.; Cahangirov, S.; Rubio, A. *Nat. Mater.* **2016**, *15* (6), 634−639.

(7) Szwacki, N. G.; Sadrzadeh, A.; Yakobson, B. I. *Phys. Rev. Lett.* **2007**, *98*, 166804.

(8) Zhai, H.-J.; Zhao, Y.-F.; Li, W.-L.; Chen, Q.; Bai, H.; Hu, H.-S.; Piazza, Z. A.; Tian, W.-J.; Lu, H.-G.; Wu, Y.-B.; Mu, Y.-W.; Wei, G.-F.; Liu, Z.-P.; Li, J.; Li, S.-D.; Wang, L.-S. *Nat. Chem.* **2014**, *6* (8), 727−731.

(9) Chen, Q.; Li, W.-L.; Zhao, Y.-F.; Zhang, S.-Y.; Hu, H.-S.; Bai, H.; Li, H.-R.; Tian, W.-J.; Lu, H.-G.; Zhai, H.-J.; Li, S.-D.; Li, J.; Wang, L.-S. *ACS Nano* **2014**, *9* (1), 754−760.

(10) Tang, H.; Ismail-Beigi, Sohrab. *Phys. Rev. Lett.* **2007**, *99* (11), 115501.

(11) Galeev, T. R.; Chen, Q.; Guo, J. C.; Bai, H.; Miao, C. Q.; Lu, H. G.; Sergeeva, A. P.; Li, S. D.; Boldyrev, A. I. *Phys. Chem. Chem. Phys.* **2011**, *13*, 11575−11578.

(12) Penev, E. S.; Bhowmick, S.; Sadrzadeh, A.; Yakobson, B. I. *Nano Lett.* **2012**, *12* (5), 2441−2445.

(13) Liu, Y.; Penev, E. S.; Yakobson, B. I. *Angew. Chem.* **2013**, *125* (11), 3238−3241.

(14) Mannix, A. J.; Zhou, X.-F.; Kiraly, B.; Wood, J. D.; Alducin, D.; Myers, B. D.; Liu, X.; Fisher, B. L.; Santiago, U.; Guest, J. R.; Yacaman, M. J.; Ponce, A.; Oganov, A. R.; Hersam, M. C.; Guisinger, N. P. *Science* **2015**, *350* (6267), 1513−1516.

(15) Feng, B.; Zhang, J.; Zhong, Q.; Li, W.; Li, S.; Li, H.; Cheng, P.; Meng, S.; Chen, L.; Wu, K. *Nat. Chem.* **2016**, *8* (6), 563−568.

(16) Feng, B.; Zhang, J.; Liu, R.-Y.; Iimori, T.; Lian, C.; Li, H.; Chen, L.; Wu, K.; Meng, S.; Komori, F.; Matsuda, I. *Phys. Rev. B: Condens. Matter Mater. Phys.* **2016**, *94* (4), 41408.

(17) Zhang, Z.; Penev, E. S.; Yakobson, B. I. *Nat. Chem.* **2016**, *8*, 525−527.

(18) Brotchie, A. *Nat. Rev. Mater.* **2016**, *1* (11), 16083.

(19) Zhang, Z.; Mannix, A. J.; Hu, Z.; Kiraly, B.; Guisinger, N. P.; Hersam, M. C.; Yakobson, B. I. *Nano Lett.* **2016**, *16* (10), 6622−6627.

(20) Li, W.-L.; Romanescu, C.; Jian, T.; Wang, L.-S. *J. Am. Chem. Soc.* **2012**, *134* (32), 13228−13231.

(21) Kiran, B.; Bulusu, S.; Zhai, H.-J.; Yoo, S.; Zeng, X. C.; Wang, L.-S. *Proc. Natl. Acad. Sci. U. S. A.* **2005**, *102* (4), 961−964.

(22) Oger, E.; Crawford, N. R. M.; Kelting, R.; Weis, P.; Kappes, M. M.; Ahlrichs, R. *Angew. Chem., Int. Ed.* **2007**, *46* (44), 8503−8506.

(23) Popov, I. A.; Jian, T.; Lopez, G. V.; Boldyrev, A. I.; Wang, L.-S. *Nat. Commun.* **2015**, *6*, 8654.

(24) Jian, T.; Li, W.-L.; Popov, I. A.; Lopez, G. V.; Chen, X.; Boldyrev, A. I.; Li, J.; Wang, L.-S. *J. Chem. Phys.* **2016**, *144* (15), 154310.

(25) Liu, M.; Artyukhov, V. I.; Lee, H.; Xu, F.; Yakobson, B. I. *ACS Nano* **2013**, *7* (11), 10075−10082.

(26) Casillas, G.; Mayoral, A.; Liu, M.; Ponce, A.; Artyukhov, V. I.; Yakobson, B. I.; Jose-Yacaman, M. *Carbon* **2014**, *66*, 436−441.

(27) Artyukhov, V. I.; Liu, M.; Yakobson, B. I. *Nano Lett.* **2014**, *14* (8), 4224−4229.

(28) La Torre, A.; Botello-Mendez, A.; Baaziz, W.; Charlier, J.-C.; Banhart, F. *Nat. Commun.* **2015**, *6*, 6636.

(29) Huang, Z.; Boulatov, R. *Chem. Soc. Rev.* **2011**, *40* (5), 2359−2384.

(30) Kresse, G.; Hafner, J. *Phys. Rev. B: Condens. Matter Mater. Phys.* **1993**, *47* (1), 558−561.

(31) Kresse, G.; Furthmüller, J. *Phys. Rev. B: Condens. Matter Mater. Phys.* **1996**, *54* (16), 11169−11186.

(32) Perdew, J. P.; Burke, K.; Ernzerhof, M. *Phys. Rev. Lett.* **1996**, *77* (18), 3865−3868.

(33) Perdew, J. P.; Burke, K.; Ernzerhof, M. *Phys. Rev. Lett.* **1997**, *78* (7), 1396.

(34) Heyd, J.; Scuseria, G. E.; Ernzerhof, M. *J. Chem. Phys.* **2003**, *118* (18), 8207−8215.

(35) Heyd, J.; Scuseria, G. E.; Ernzerhof, M. *J. Chem. Phys.* **2006**, *124* (21), 219906−219906−1.

(36) Blöchl, P. E. *Phys. Rev. B: Condens. Matter Mater. Phys.* **1994**, *50* (24), 17953.

(37) Kresse, G.; Joubert, D. *Phys. Rev. B: Condens. Matter Mater. Phys.* **1999**, *59* (3), 1758−1775.

DOI: 10.1021/jacs.6b12750
J. Am. Chem. Soc. 2017, 139, 2111−2117

(38) Henkelman, G.; Uberuaga, B. P.; Jónsson, H. *J. Chem. Phys.* **2000**, *113* (22), 9901−9904.
(39) Aradi, B.; Hourahine, B.; Frauenheim, T. *J. Phys. Chem. A* **2007**, *111* (26), 5678−5684.
(40) Grundkötter-Stock, B.; Bezugly, V.; Kunstmann, J.; Cuniberti, G.; Frauenheim, T.; Niehaus, T. A. *J. Chem. Theory Comput.* **2012**, *8* (3), 1153−1163.
(41) Cretu, O.; Komsa, H.-P.; Lehtinen, O.; Algara-Siller, G.; Kaiser, U.; Suenaga, K.; Krasheninnikov, A. V. *ACS Nano* **2014**, *8* (12), 11950−11957.
(42) Li, D.-Z.; Chen, Q.; Wu, Y.-B.; Lu, H.-G.; Li, S.-D. *Phys. Chem. Chem. Phys.* **2012**, *14* (43), 14769−14774.
(43) Bai, H.; Chen, Q.; Miao, C.-Q.; Mu, Y.-W.; Wu, Y.-B.; Lu, H.-G.; Zhai, H.-J.; Li, S.-D. *Phys. Chem. Chem. Phys.* **2013**, *15* (43), 18872−18880.
(44) Peierls, R. E. *Ann. Phys.* **1930**, *4* (2), 121−148.
(45) Peierls, R. E. *Quantum Theory of Solids*; Clarendon Press: Oxford, 2001.
(46) Frohlich, H. *Proc. R. Soc. London, Ser. A* **1954**, *223* (1154), 296−305.
(47) Kennedy, T.; Lieb, E. H. *Phys. Rev. Lett.* **1987**, *59* (12), 1309−1312.
(48) Kertesz, M.; Koller, J.; Azman, A. *J. Chem. Phys.* **1978**, *68* (6), 2779−2782.
(49) Bylaska, E. J.; Weare, J. H.; Kawai, R. *Phys. Rev. B: Condens. Matter Mater. Phys.* **1998**, *58* (12), R7488−R7491.
(50) Roark, R. J.; Young, W. C.; Budynas, R. G.; Sadegh, A. M. *Roark's Formulas for Stress and Strain*, 8th ed.; McGraw-Hill: New York, 2012.
(51) Dumitrica, T.; Hua, M.; Yakobson, B. I. *Proc. Natl. Acad. Sci. U. S. A.* **2006**, *103* (16), 6105−6109.
(52) Litters, S.; Kaifer, E.; Enders, M.; Himmel, H.-J. *Nat. Chem.* **2013**, *5* (12), 1029−1034.
(53) Tongay, S.; Durgun, E.; Ciraci, S. *Appl. Phys. Lett.* **2004**, *85* (25), 6179−6181.

DOI: 10.1021/jacs.6b12750
J. Am. Chem. Soc. 2017, 139, 2111−2117